Journal of Applied Fluid Mechanics, Vol. 11, No. 6, pp. 1557-1568, 2018.
Available online at www.jafmonline.net, ISSN 1735-3572, EISSN 1735-3645.
DOI: 10.29252/jafm.11.06.28883

Lubricant Rheological Behavior Effect Analysis on the Performance of Finite Porous Self- Lubricating Journal Bearings

M. Malki[1], S. Larbi[1†], S. Boubendir[2] and R. Bennacer[3]

[1] *LGMD, Polytechnic National School of Algiers 1, 10, Avenue Hassen Badi, Algiers, Algeria*
[2]*USTHB, BP 32, El Alia, 16111 Bab Ezzouar, Algiers, Algeria*
[3]*L. M. T – E. N. S. Cachan. Paris - France*

†*Corresponding Author Email: salah.larbi@g.enp.edu.dz*

(Received February 13, 2018; accepted April 21, 2018)

ABSTRACT

In this paper, the hydrodynamic lubrication of finite porous self-lubricating journal bearings is investigated taking into account the rheological lubricant behavior effect. The modified Reynolds equation is derived by considering both the fluid flow in the porous matrix and the lubricant rheological behavior where Darcy's law and power- law model were used. Governing differential equations were solved numerically using the finite difference method. Static characteristics are obtained by considering three types of lubricants: pseudo-plastic, dilatant and Newtonian fluids. Obtained results showed that the power law index, n, has important effects on the performance of porous and non-porous bearings. An improvement in the fluid bearing characteristics (load capacity, pressure) is observed for dilatant fluids (n>1) while these characteristics decreased for pseudo-plastic fluids (n<1). The permeability of the porous structure has significant effects on the performance of porous journal bearings of finite length, particularly at higher eccentricity ratios. Good agreement is observed between the results obtained in this study and those of literature revue.

Keywords: Hydrodynamic lubrication; Porous journal bearing; Non-Newtonian fluid; Power law.

NOMENCLATURE

C	radial clearance
e	eccentricity
D	bearing diameter
h	film thickness
K	permeability
k	dimensionless permeability
L	length bearing
m	power law consistency coefficient
n	power law index
P	pressure
Q	load capacity
R	radius
u,v,w	velocity components
x,y,z	space coordinates
Ω	over-relaxation parameter

Greek Symbols

ε	eccentricity ratio
ε_{ij}	components of the rate deformation tensor
ϕ	attitude angle
η	dimensional ratio
μ	dynamic viscosity
θ	angular coordinate
ρ	fluid density
ω	angular velocity of the journal

Superscripts

¯	dimensional variables
*	porous

Subscripts

b	bush
e	external surface
s	shaft

1. INTRODUCTION

Journal bearings are encountered in many industrial applications. In mechanical construction, they are used to lift and guide the shafts in rotation. The development of lubricants has become an integral part of the development of machinery and its corresponding technologies where they are considered to be a reliable element in increasing the

machinery lifetime and in improving its mechanical properties (Mishra (2013)).

The principal advantage of porous journal bearings is that they can be used in areas where the conventional bearings are unusable such as in situations of congestion and inaccessibility for lubrication and, in applications where contamination is intolerable such as in agro-food and textile industries. They operate silently and without maintenance, their cost is considerably less expensive than externally lubricated bearings (Boubendir *et al*. (2010)).

During its motion, the oil is sucked in shaft rotation to lubricate the contact, and is reabsorbed by the bearing bushing when stationary. At the start-up, the contact bearing-shaft is never dry, unlike a conventional bearing, by avoiding bearing wear. In their operating mode, Braun (1982) noted that the pressure difference at the bearing surface created by the shaft rotation will ensure circulation and supply of oil.

Cameron and Morgan (1957) were the first authors in conducting a comprehensive study by developing a mathematical model for investigating the lubrication in porous bearings. The recent studies on porous bearings, or most of them, conducted by Elsharkawy and Guedouar (2001), Naduvinamani and Santosh (2011), Balasoiu *et al*. (2013) were devoted to the study of hydrodynamic lubrication and the determination of journal bearing characteristics for different variables: eccentricity, permeability, boundary conditions. These studies have shown that the increase in the permeability generates a decrease in the characteristics of the bearings: load capacity, pressure. Experimental results of Mokhtar *et al*. (1984) have confirmed these results.

Basically, these studies are focused on the porous bearings characteristics lubricated with a Newtonian fluid, where the stress tensor is directly proportional to the strain one. This assumption is not a satisfactory approach for many lubricant fluids where the pressure gradient is large and the shear rate is high.

The widespread use of non-Newtonian fluids as lubricants in mechanical engineering applications is a consequence of the improvement of the lubricants quality and then the reduction of friction and wear. Several theoretical developments have been achieved during these last decades to describe the non-Newtonian lubricant behavior of fluids. Some of them have been successfully applied in lubrication problems based on power- law model by Jang and Chang (1988), Prasad and Chhabra (1991), Chu *et al*. (2006), Nessil *et al*. (2013).

In many engineering applications, Wang *et al*. (1987), Bhattacharjee and Das (1996) demonstrated that the fluid lubricants are frequently described by the power law model such as pseudo-plastic ($n<1$) and dilatant ($n>1$) fluids which are two important classes of non-Newtonian lubricants.

Sinha and Singh (1981) analyzed the behavior of spherical bearings lubricated with a non-Newtonian fluid described by the power-law model. They showed that the bearing load carrying capacity increased with the increase in the power law index. Rodin (1996) revised the previous study of Sinha and Singh (1981) for the thin film case. The author demonstrated that their solution was only valid for $n\geq⅓$, where the resistance to the fluid motion is dominated by the flux in the film.

Chu *et al*. (2006) presented a comprehensive study based on the modified Reynolds equation 1-D where a power-law model for thin film elasto-hydrodynamic lubrication is used. They found that the power law index, n, affects significantly the pressure distribution. The higher is the flow index, the higher is the pressure peak.

Lin *et al*. (2016) conducted studies on Newtonian lubricants with adding substances (polymer thickened oils, viscosity index improvers, poly-isobutylene). They analyzed dilatant and pseudo-plastic properties on the basis of the Rabinowitsch flow model. The authors noted that the non-Newtonian behavior of the dilated lubricants gives higher values of the load carrying capacity and the friction parameter. The non-Newtonian properties of pseudo-plastic fluids provides opposite values.

Lin and Wang (1990) analyzed the thermo-hydrodynamic case for a finite-dimensional partial bearing, using non-Newtonian lubricants and following the power- law model. The energy equation, including convective and viscous dissipation terms, is coupled with Reynolds equation to solve the temperature variation in the fluid film. The obtained results showed an improvement in the load capacity and pressure using dilatant fluids.

Mongkolwongrojn *et al*. (2010) have studied the effects of the surface roughness and the rheological behavior of lubricants on the stability of a rigid rotor under TEHL (thermal elasto-hydazrodynamic lubrication) lubrication using non-Newtonian fluid described by Carreau viscosity model. They showed that the stability of the bearing system deteriorates with the decrease of both the power law index and the elastic modulus of bearing liner material.

The work conducted by Jang and Chang (1987) demonstrated that the load capacity, the maximum of temperature and the friction force can be greatly increased using dilatant lubricants ($n>1$). For pseudo- plastic fluids ($n<1$), they observed opposite results.

Ju *et al*. (1994) analyzed the thermo-hydrodynamic aspect of a finite width hydrodynamic journal bearing using non-Newtonian lubricants. The used lubricants are described by the power-law model. The modified Reynolds equation is solved numerically by using Elrod algorithm. The authors showed that the thermal effects are more pronounced at higher values of power law index, n.

Kango *et al*. (2014) analyzed the combined influence of viscous heat dissipation and non-Newtonian rheological behavior of lubricants on the

performance parameters of micro-textures of bearings. The high value of the power law index (n=1.1) gives a maximum increase in the load carrying capacity (about 10%). The micro texture provides improved bearing performance parameters for low eccentricity ratios.

A numerical solution for the hydrodynamic lubrication of a magnetic head-rigid disk lubricated with a power-law fluid was performed by Elsharkawy (2001). The results showed that the power-law exponent has a significant effect on the pressure profile and load carrying capacity.

Sakim, *et al.* (2018) studied numerically the influence of the couple stresses on finite porous elastic journal bearing performance. The authors showed that the couple stresses increase the load capacity and decreased the friction factor.

The bearing deformation reduces these quantities, especially, when such bearings operate at high eccentricities.

As far as we know, based on the literature review, no comprehensive study has been done using the combined effects of the porous bush and the non-Newtonian lubricant fluid behavior in hydrodynamic lubrication case of finite porous journal bearings using 3-D model. The main aim of this paper is to illustrate the lubricant rheological behavior effects, based on the power- law model, on the finite porous journal bearing static characteristics. The present study is devoted to the hydrodynamic lubrication analysis based on modified Reynolds equation taking into account the non-Newtonian fluid behavior and Darcy's law for fluid flow in the porous matrix. The effects of the permeability and eccentricity ratio on the journal bearing performances, the pressure, the load carrying capacity and attitude angle are presented and analyzed.

2. PHYSICAL AND MATHEMATICAL MODELS

Figure 1 shows the median section of a cylindrical porous bearing. The considered bearing consists of a porous bush of center O_b, with internal radius R_b and external radius Re and a shaft with center O_s and radius R_s. Under the load action, the centers O_b and O_s do not coincide. The journal rotates with a constant angular velocity about its axis.

The angle between the line of centers O_sO_b and the direction of the load is the attitude angle ϕ. We can then calculate the position of the shaft in the bush. Since the radius R_b and R_s are practically identical ($(R_b-R_s)/R_b \approx 0{,}001$), the curvature of the film can be neglected and by developing the bush and film the problem can be assimilated as a plane problem. Figure 2 shows the simplified schematics of the developer bearing.

Following to the above assumptions, the film thickness is given by the expression:

$$h = C\,(1 + \varepsilon \cos\theta) \tag{1}$$

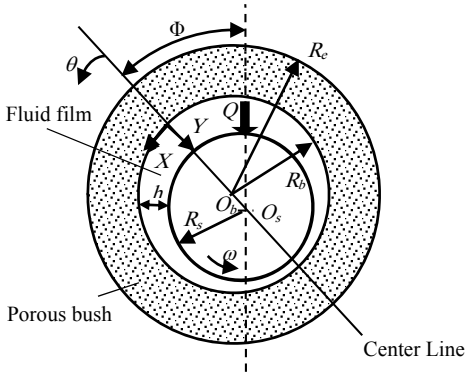

Fig. 1. Schematic representation of a journal bearing.

$$\text{Where: } \begin{cases} \varepsilon = \dfrac{e}{C} \\ C = R_b - R_s \\ \theta = \dfrac{x}{R_s} \end{cases} \tag{2}$$

In Cartesian coordinates system, as it is seen in Fig. 2, the "XOZ" plane coincides with the developed surface.

By considering Darcy's law which characterizes the fluid flow in the porous domain, the boundary conditions on the velocities for the bush are:

$$U_1 = -\frac{K}{\mu_b}\frac{\partial P^*}{\partial x}\bigg|_{R=R_b} \tag{3}$$

$$V_1 = -\frac{K}{\mu_b}\frac{\partial P^*}{\partial R}\bigg|_{R=R_b} \tag{4}$$

$$W_1 = -\frac{K}{\mu_b}\frac{\partial P^*}{\partial z}\bigg|_{R=R_b} \tag{5}$$

For the fluid-shaft interface, the velocity components are:

$$U_2 = U(\theta, h, z) = \omega R_s \tag{6}$$

$$V_2 = V(\theta, h, z) = \omega\frac{dh}{d\theta} \tag{7}$$

$$W_2 = W(\theta, h, z) = 0 \tag{8}$$

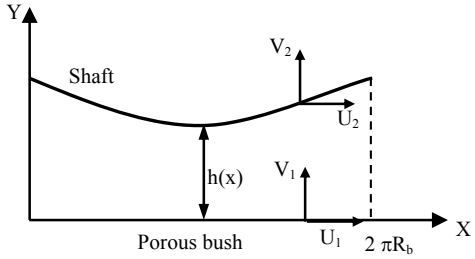

Fig. 2. Simplified schematics of the developer bearing.

In the porous journal bearing, the fluid flows in two domains: the porous bush and the lubricating film. The mathematical modeling of the problem is based on the understanding of the fluid flow in the porous matrix and in the lubricating film as well as the boundary conditions at the interface between the two mediums.

2.1 Power Law of Non-Newtonian Fluid Behavior

The expression of the generalized viscosity for an

incompressible fluid in the power-law model is used by Vijaysri and Chhabra (1999), Al-Fadhalah and Elsharkawy (2008):

$$\mu = m\,(2\,\Pi)^{\frac{(n-1)}{2}} \tag{9}$$

Π, is the second invariant of the deformation rate tensor given by:

$$\Pi = \sum_i \sum_j \varepsilon_{ij}\varepsilon_{ji} \tag{10}$$

Depending on the value of «n», three types of fluids can be distinguished:

- For: n=1, the fluid behavior is Newtonian.
- For: n>1, the fluid behavior is dilatant.
- For: n<1, the fluid behavior is pseudo-plastic.

2.2 Reynolds Generalized Equation

The generalized Reynolds equation applied to a porous bearing using a non-Newtonian fluid is deduced from equations of viscous thin films, which are given by the equations of the mechanics of the continuous media. Governing equations describing the physical phenomena are established, by assuming some simplifying assumptions:

- The thickness of the lubricating film is too small compared to the other dimensions of the bearing.

- The shaft and the bush are non deformable.

- The fluid is non-Newtonian and incompressible.

- The flow is laminar, and the porous medium is homogeneous and isotropic.

Taking into account the geometric and velocity conditions defined above, the generalized Reynolds equation is given by Boubendir *et al*. (2011):

$$\frac{\partial}{\partial x}\left[\left(G+\frac{K\,F}{\mu}\right)\frac{\partial P}{\partial x}\right] + \frac{\partial}{\partial z}\left[\left(G+\frac{K\,F}{\mu}\right)\frac{\partial P}{\partial z}\right]$$

$$= \omega\,R_s\frac{\partial}{\partial x}(\rho\,h - F) - \rho\frac{K}{\mu}\frac{\partial P^*}{\partial R}\Big|_{R=R_b} \tag{11}$$

Where:

$$G = \int_0^H \frac{Ry}{\mu}dy - I_2\,F\,;\quad F = \frac{1}{J_2}\int_0^H \frac{\rho y}{\mu}dy$$

$$I_2 = \int_0^H \frac{y}{\mu}dy\,;\; J_2 = \int_0^H \frac{dy}{\mu} \tag{12}$$

The components of the velocity u, and w, are:

$$\begin{cases} u = \dfrac{\partial P}{\partial x}(I - J\,F) + \dfrac{u_2 - u_1}{J_2}J + u_1 \\ w = \dfrac{\partial P}{\partial z}(I - J\,F) + \dfrac{w_2 - w_1}{J_2}J + w_1 \end{cases} \tag{13}$$

Where:

$$I = \int_0^y \frac{\xi}{\mu}d\xi,\; J = \int_0^y \frac{d\xi}{\mu} \tag{14}$$

The fluid flow in the porous domain is governed by Darcy's law (1856). Combined with the continuity equation, we obtain:

$$\frac{1}{R}\frac{\partial}{\partial R}\left(\frac{R}{\mu_b}\frac{\partial P^*}{\partial R}\right) + \frac{1}{R^2}\frac{\partial}{\partial\theta}\left(\frac{1}{\mu_b}\frac{\partial P^*}{\partial\theta}\right) + \frac{\partial}{\partial z}\left(\frac{1}{\mu_b}\frac{\partial P^*}{\partial z}\right) = 0 \tag{15}$$

The above equations are second-order partial differential equations of elliptic type where the main unknown parameter is the pressure.

2.3 Dimensionless Form of Equations

To generalize the study, consider the dimensionless parameters defined as follow:

$$\bar{P} = \frac{PC^2}{\mu_0\omega R_s R_b};\; \bar{R} = \frac{R}{R_b};\; \bar{h} = \frac{h}{C};\; \bar{k} = \frac{KR_b}{C^3};$$

$$\bar{C} = \frac{C}{R_b};\; \theta = \frac{x}{R_b};\; \bar{y} = \frac{y}{h};\; \bar{z} = \frac{z}{L};\; \eta = \frac{R_b}{L} \tag{16}$$

$$(\bar{u}, \bar{v}, \bar{w}) = \frac{(u,v,w)}{\omega R_s}\;;\; \bar{\mu} = \frac{\mu}{\mu_0} \tag{17}$$

The above Eqs. (11-15) become:

$$\frac{\partial}{\partial\theta}\left[\left(\bar{h}^3\bar{G} + \frac{\bar{k}\bar{C}\bar{h}\bar{F}}{\bar{\mu}}\right)\frac{\partial\bar{P}}{\partial\theta}\right] + \eta^2\frac{\partial}{\partial\bar{z}}\left[\left(\bar{h}^3\bar{G} + \frac{\bar{k}\bar{C}\bar{h}\bar{F}}{\bar{\mu}}\right)\frac{\partial\bar{P}}{\partial\bar{z}}\right]$$

$$= \frac{\partial}{\partial\theta}\left[\bar{h}(1-\bar{F})\right] - \frac{\bar{k}}{\bar{\mu}}\frac{\partial\bar{P}^*}{\partial\bar{R}}\Big|_{\bar{R}=1} \tag{18}$$

$$\frac{1}{\bar{R}}\frac{\partial}{\partial\bar{R}}\left(\frac{\bar{R}}{\bar{\mu}_b}\frac{\partial\bar{P}^*}{\partial\bar{R}}\right) + \frac{1}{\bar{R}^2}\frac{\partial}{\partial\theta}\left(\frac{1}{\bar{\mu}_b}\frac{\partial\bar{P}^*}{\partial\theta}\right) +$$

$$\eta^2\frac{\partial}{\partial\bar{z}}\left(\frac{1}{\bar{\mu}_b}\frac{\partial\bar{P}^*}{\partial\bar{z}}\right) = 0 \tag{19}$$

The velocity components will be:

$$\begin{cases} \bar{u} = \dfrac{\partial\bar{P}}{\partial\theta}\left[\bar{h}^2(\bar{I} - \bar{J}\bar{F}) + \dfrac{\bar{k}\bar{C}}{\bar{\mu}_b}\left(\dfrac{\bar{J}}{\bar{J}_2} - 1\right)\right] + \dfrac{\bar{J}}{\bar{J}_2} \\ \bar{w} = \eta\dfrac{\partial\bar{P}}{\partial\bar{z}}\left[\bar{h}^2(\bar{I} - \bar{J}\bar{F}) + \dfrac{\bar{k}\bar{C}}{\bar{\mu}_b}\left(\dfrac{\bar{J}}{\bar{J}_2} - 1\right)\right] \end{cases} \tag{20}$$

2.4 Boundary Conditions

The resolution of both Reynolds equations and pressure equation in the porous medium requires the knowledge of boundary conditions reflecting the physical reality.

2.4.1 In the Fluid Film

On the circumferential direction and edges of the bearing, we have:

$$\begin{cases} \bar{P}\left(\theta, \mp\frac{1}{2}\right) = 0 \\ \bar{P}(0,\bar{z}) = \bar{P}(2\,\pi,\bar{z}) \end{cases} \tag{21}$$

The cavitation zone was characterized by Swift (1932) and Stieber (1933). The corresponding conditions are:

$$\bar{P}(\theta_c) = 0\;;\; \frac{\partial\bar{P}}{\partial\theta}(\theta_c) = 0 \tag{22}$$

2.4.2 At the Interface Fluid Film-Porous Bush

The corresponding boundary conditions are those of continuity of pressure and velocities at the interface fluid film- porous bush given by:

$$\bar{P}^*(\theta, \bar{R}_b, \bar{z}) = \bar{P}(\theta,\bar{z}) \tag{23}$$

2.4.3 In the Porous Bush

The pressure in the close bearing (pore sealed) and circumferential direction is given by:

$$\begin{cases} \dfrac{\partial \overline{P}^*}{\partial \overline{R}}(\theta, \overline{R}_e, \overline{z}) = 0 \\ \overline{P}^*(0, \overline{R}, \overline{z}) = \overline{P}^*(2\pi, \overline{R}, \overline{z}) \\ \dfrac{\partial \overline{P}^*}{\partial \overline{z}}\left(\theta, \overline{R}, \mp\dfrac{1}{2}\right) = 0 \end{cases} \quad (24)$$

2.5 Load Capacity and Attitude Angle

The load capacity and the attitude angle are obtained by integrating the pressure field on the surface of the journal bearing. At equilibrium, we have:

$$\overline{Q} = \frac{Q}{\mu_0 \omega R_b^3 L/C^2} = \sqrt{\overline{Q}_L^2 + \overline{Q}_K^2} \quad (25)$$

$$\tan\phi = -\overline{Q}_L/\overline{Q}_K \quad (26)$$

Where:

$$\overline{Q}_L = \int_{-½}^{½}\int_0^{2\pi} \overline{P}\,\mathrm{Sin}\theta\, d\theta\, d\overline{z} \quad (27)$$

$$\overline{Q}_K = \int_{-½}^{½}\int_0^{2\pi} \overline{P}\,\mathrm{Cos}\theta\, d\theta\, d\overline{z} \quad (28)$$

3. NUMERICAL PROCEDURE

The governing equations of fluid flow (Reynolds equation in the fluid film and Darcy' law in the porous medium) are differential equations of elliptic type. Their resolution (taking into account the effect of the variation of the viscosity of the fluid) is quite complex and requires the use of numerical iterative computation. For this purpose, the finite difference scheme was used to discretize these equations. The discretized form of Reynolds equation by finite difference method is given by:

$$\overline{P}_{i,k} = \Omega\left[A_1\overline{P}_{i+1,k} + A_2\overline{P}_{i-1,k} + A_3\overline{P}_{i,k+1} + A_4\overline{P}_{i,k-1} + A_5\right] + (1-\Omega)\overline{P}_{i,k} \quad (29)$$

Where: Ai (i=1,5), are the equation coefficients.

The resolution of this system is obtained using Gauss Seidel's iterative method with over-relaxation parameter, Ω, which is equal to 1.8.

The use of an iterative method for numerical resolution is justified by the application of Reynolds boundary conditions.

The pressure is the only unknown parameter in the calculation, once the eccentricity is given.

The application of this method to Darcy's equation makes it possible to obtain the system of linear equations:

$$\overline{P}^*_{i,j,k} = \Omega\left[B_1\overline{P}^*_{i+1,j,k} + B_2\overline{P}^*_{i-1,j,k} + B_3\overline{P}^*_{i,j+1,k} + B_4\overline{P}^*_{i,j-1,k} + B_5\overline{P}^*_{i,j,k+1} + B_6\overline{P}^*_{i,j,k-1}\right] + (1-\Omega)\overline{P}^*_{i,j,k} \quad (30)$$

Where: Bi (i=1, 6), are the equation coefficients.

The flow chart of Fig. 3 illustrates the detail of the computational procedure.

The discretized generalized Reynolds equation in the fluid film and Darcy's discretized equation in the bush are solved numerically and simultaneously. The equality of velocities and pressures at the fluid film-bush interface will be taken into account during the iterative process. The cavitation zone is determined numerically by using Christopherson's method (1941).

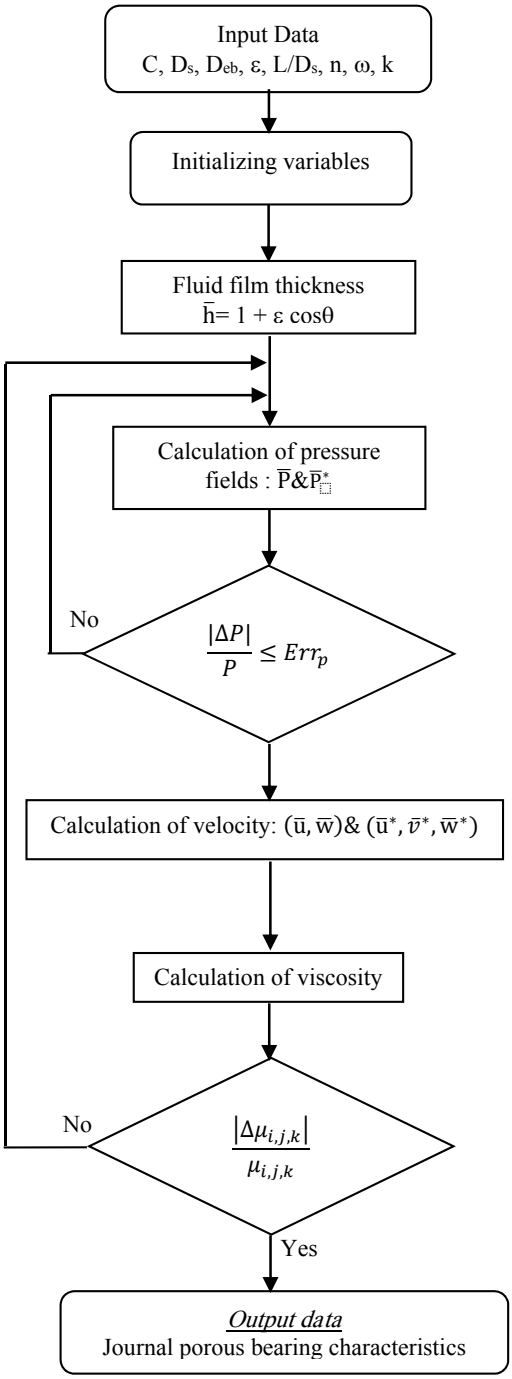

Fig. 3. Calculation flow chart for the case study.

The corresponding convergence criterion for the various parameters is:

$$\frac{|\overline{P}^{new} - \overline{P}^{old}|}{\overline{P}^{old}} \le 10^{-3} \text{ and } \frac{|\overline{\mu}^{new} - \overline{\mu}^{old}|}{\overline{\mu}^{old}} \le 10^{-3}.$$

4. RESULTS AND DISCUSSIONS

Based on the governing equations described previously, a computer program was developed to study the performance of the self- lubricating finite

porous hydrodynamic journal bearing using non-Newtonian lubricants. In order to demonstrate the validity of the present analysis as well as the developed computational code, extensive comparisons with the results available in the literature have been conducted by Ju *et al.* (1994) and Mokhtar *et al.* (1984).

Figure 4 illustrates the comparison between the numerical results obtained in this study and those of Ju *et al.* (1994) for a non-porous journal bearing case. These results are related to the dimensionless load versus the eccentricity ratio. The figure shows good agreement between the different results for the three types of considered lubricants (pseudo-plastic, Newtonian and dilatant fluids).

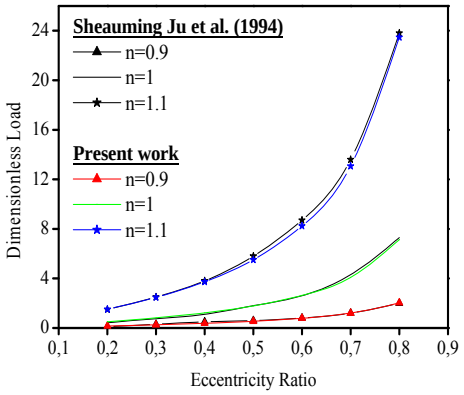

Fig. 4. Evolution of load capacity versus eccentricity. Results comparison with Ju *et al.* results (1994).

Figure 5 shows the comparison of the dimensionless load capacity versus the relative eccentricity between our results and experimental data of Mokhtar *et al.* (1984). As it is illustrated in the figure, good agreement is observed between our numerical results and experimental data of Mokhtar *et al.* (1984). However, the slight difference observed between the different results, for high eccentricity ratios, may be due to the fact that thermal effects are neglected in the mathematical modeling.

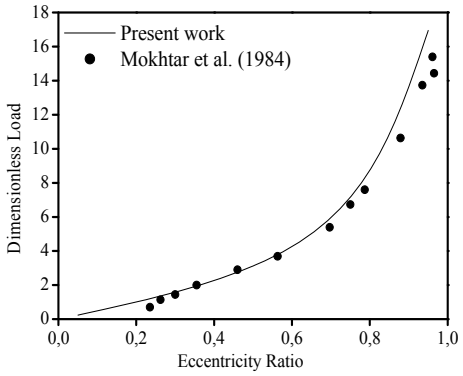

Fig. 5. Evolution of load capacity versus eccentricity. Comparison with experimental data of Mokhtar *et al.* (1984).

Technical data used in the numerical simulation for the results presented in this study (sealed self porous smooth journal bearing case) are listed in Table 1.

Table 1 Technical data used in the numerical simulation.

Shaft diameter, D_s	100 mm
External bush diameter, D_{eb}	200 mm
Length bearing, L	100 mm& 300 mm
Radial clearance, C	100µm
Revolution speed	2000 rev/min
Relative eccentricity, e/C	0.7
Dimensionless permeability, k	$0 - 10^{-1}$
Power law index, n	0.9, 1, 1.1

Figures 6, 7 and 8, 9 represent respectively the dimensionless pressure variation of the lubricating fluid film in the median plane position of the bearing versus the circumferential coordinates and axial direction.

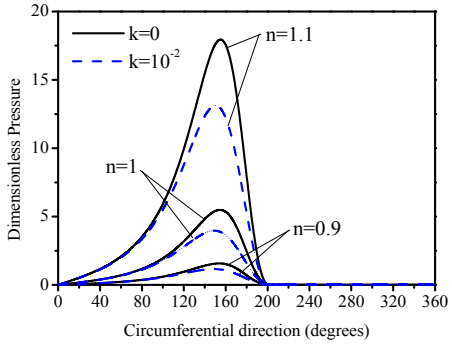

Fig. 6. Evolution of pressure versus circumferential direction and function of the power law index and permeability for: $L/D_s=1$.

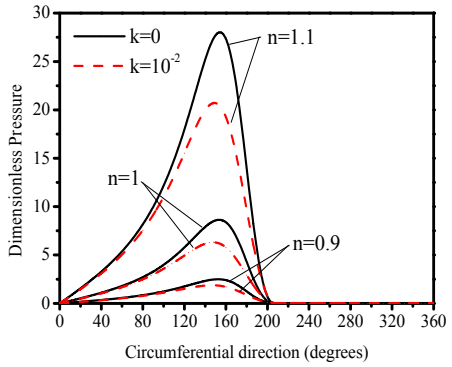

Fig. 7. Evolution of pressure versus circumferential direction and function of the power law index and permeability for: $L/D_s=3$.

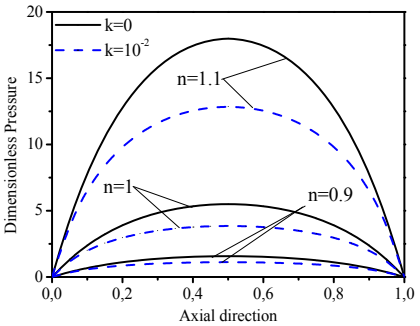

Fig. 8. Evolution of pressure versus axial direction and function of the power law index and permeability at the plane θ =160° for: $L/D_s=1$.

The results are related to different values of permeability and power law index for two values of L/D_s. The figures show the existence of a pressure, concentrated in the middle of the bearing and corresponding to an angular position of 160°. It should be noted that the increase in the power law index, n, generates a considerable hydrodynamic pressure. The comparison between Figs. 6, 7, 8 and 9, highlights the proportionally character between the pressure peak and L/D_s ratio.

Figures 10 and 11 illustrate the evolution of the dimensionless maximum pressure versus the relative eccentricity for a power law indexes equal to 0.9, 1 and 1.1. The results are for two values of L/D_s ratio and in porous and non-porous bearing cases.

The comparison between Figs. 10 and 11 shows that the value of the pressure peak is proportional to L/D_s ratio. The profile of the maximum pressure versus the non-dimensional permeability for the same values of the power law index, n, is shown in Fig. 12.

All these figures demonstrate that the increase in the power law index, n, generates a significant increase in pressure. The increase in the permeability generates a decrease in the pressure from a critical value of the dimensionless permeability which is equal to 10^{-3}. In addition, it can be noted that the pressure increases with the increase in the relative eccentricity.

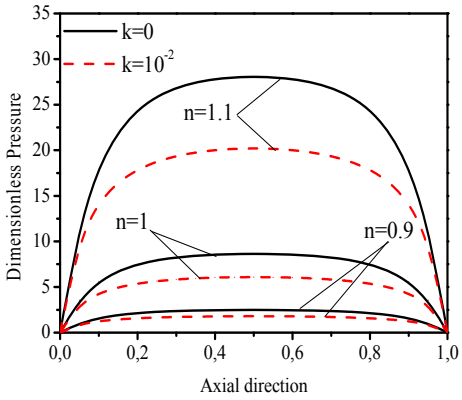

Fig. 9. Evolution of pressure versus axial direction and function of the power law index and permeability at the plane θ =160° for: L/D_s=3.

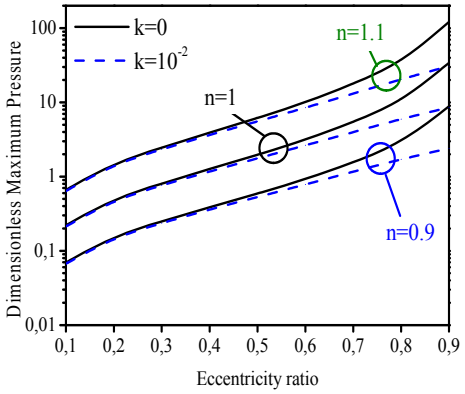

Fig.10. Evolution of the maximum pressure versus eccentricity ratio for different values of power law index and permeability for: L/D_s=1.

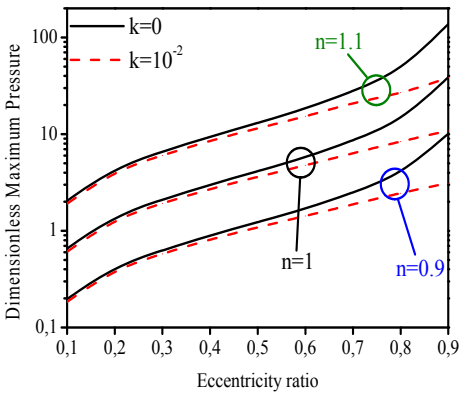

Fig. 11. Evolution of the maximum pressure versus eccentricity ratio for different values of power law index and permeability for: L/D_s=3.

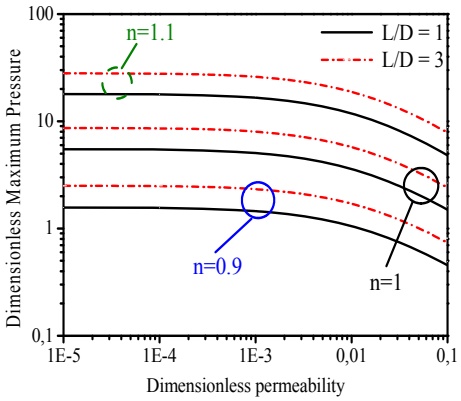

Fig. 12. Evolution of the maximum pressure versus permeability for different values of power law index and permeability.

Figures 13 and 14 depict the variation of the load capacity function of the relative eccentricity for different values of the power law index and L/D_s ratio and, for porous and non-porous bearing cases.

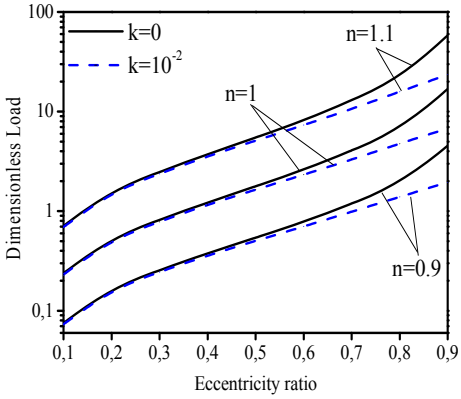

Fig. 13. Evolution of load capacity versus the eccentricity ratio for different values of power law index and permeability for: L/D_s=1.

The variation of the load capacity function of permeability for power law indexes equal to 0.9, 1 and 1.1 and, for two values of L/D_s ratio is shown in Fig. 15. In all figures, a considerable increase of load capacity with dilatant fluids (n>1) is observed. This increase becomes significant with the increase in relative eccentricity and L/D_s ratio, for non-

porous journal bearing cases. It can also be noted that the load capacity decreases with the increase of the permeability from a critical value of the dimensionless permeability whose value is 10^{-3}.

The comparison between Figs.13, 14 and 15 shows that the value of the load capacity is proportional to L/D_s ratio. It can also be noted that the use of dilatant fluids can compensate the degradation of the load capacity which is generated by the presence of the porous matrix. As it can be seen in Figs 13, 14 and 15, the dimensionless load capacity of a porous bearing with a power law index value, n=1.1, is greater than a Newtonian non porous bearing.

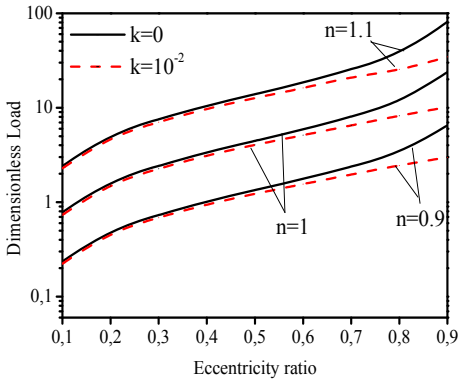

Fig. 14. Evolution of load capacity versus the eccentricity ratio for different values of power law index and permeability for: L/D_s=3.

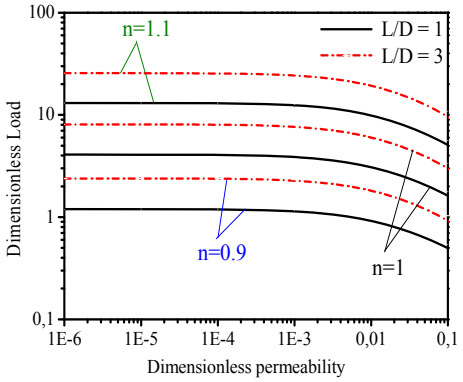

Fig. 15. Evolution of load capacity versus permeability for different values of power law index and L/D_s.

Figure 16 shows the evolution of the attitude angle versus permeability for different values of power law index and L/D_s which is equal to 1 and 3. Figures 17 and 18 illustrate the variation of the attitude angle versus the relative eccentricity for different values of the power law index and for two values of L/D_s ratio in porous and non-porous bearing cases. Notice in Fig. 16 that the increase in L/D_s ratio generates an increase in the attitude angle.

It can be seen from these figures that the attitude angle is inversely proportional to the power law index, n, and the relative eccentricity. In addition, the attitude angle increases with increasing permeability from approximately a critical value of 10^{-4}. The power law index, n, has not a great influence on the attitude angle for small eccentricities. The pseudo-plastic fluid has a larger attitude angle for the greatest permeability and for L/D_s=3.

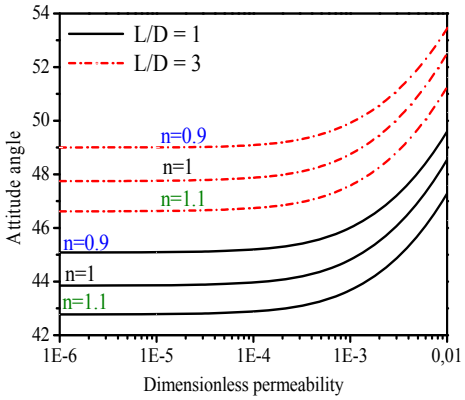

Fig. 16. Evolution of the attitude angle versus permeability for different values of power law index and L/D_s.

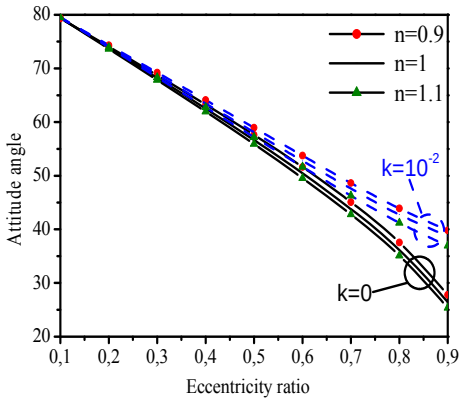

Fig. 17. Evolution of the attitude angle versus eccentricity ratio for different values of power law index and permeability for: L/D_s=1.

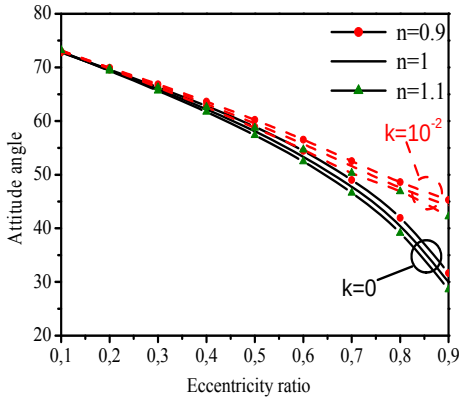

Fig. 18. Evolution of the attitude angle versus eccentricity ratio for different values of power law index and permeability for: L/D_s=3.

The friction coefficient is defined as the ratio of the friction force to the hydrodynamic load capacity. The evolution of this coefficient versus the eccentricity ratio is presented in Figs. 19 and 20 for two values of L/D_s which are equal to 1 and 3 and for a power law index of 0.9, 1 and 1.1, in porous and non-porous journal bearing cases.

It can be noted that the friction coefficient decreases with the increase in the power law index, n, and eccentricity. This decrease becomes more appreciable for large eccentricities in non-porous bearing cases. It can also be underlined that the friction parameter is proportional to the permeability. The comparison between Figs. 19 and 20 shows that the values of the friction coefficient for $L/D_s=3$ are smaller than those for $L/D_s=1$.

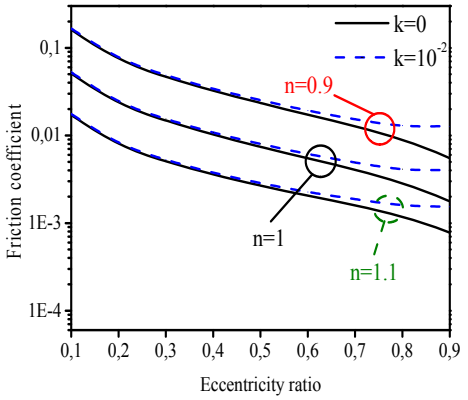

Fig. 19. Variation of the friction coefficient versus eccentricity ratio for different values of power law index and permeability for: $L/D_s=1$.

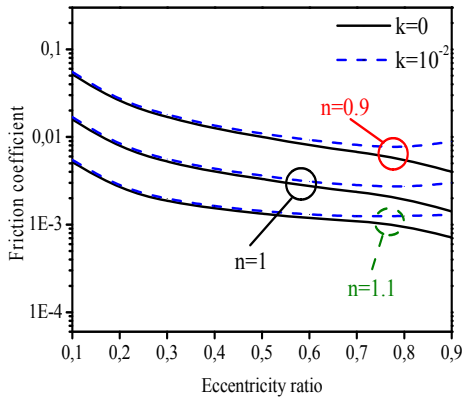

Fig. 20. Variation of the friction coefficient versus eccentricity ratio for different values of power law index and permeability for: $L/D_s=3$.

Figure 21 illustrates the evolution of the load capacity versus power law index, n, for two values of permeability (porous and non-porous bearing cases) and two eccentricity ratios with L/D_s equal to 1. The figure confirmed that the increase of power law index, n, generates high load capacity for all cases. Notice that considerable increasing of load capacity is observed for non-porous bearing and for high relative eccentricity cases.

The variation of the friction coefficient versus the power law index, n, for two values of permeability and two eccentricity ratios for porous and non-porous bearing cases and L/D_s equal to 1 is shown in Fig. 22. The figure illustrates that the increase of power law index, n, reduces the friction coefficient for porous and non-porous bearings for two cases of eccentricity. Notice that the low friction coefficient value is observed for non-porous journal bearing case and high eccentricity.

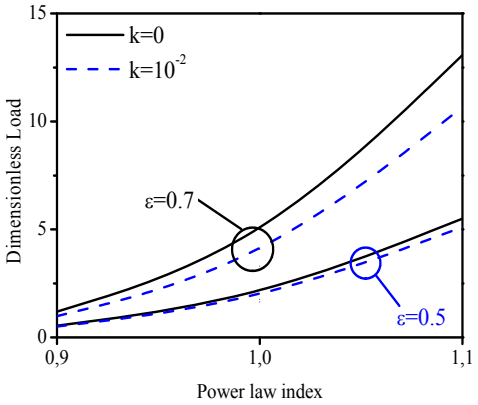

Fig. 21. Evolution of load capacity versus power law index, n, for two values of permeability and eccentricity ratio for: $L/D_s=1$.

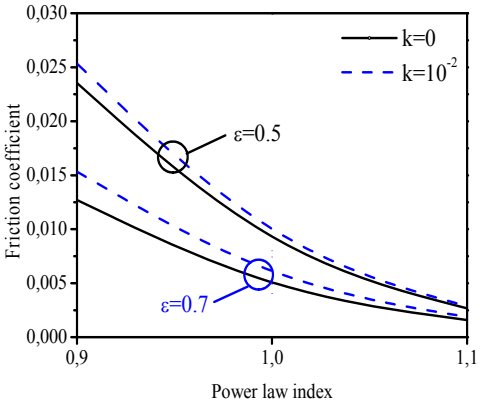

Fig. 22. Variation of the friction coefficient versus power law index, n, for two values of permeability and eccentricity ratio for: $L/D_s=1$.

Figures 23, 24 and 25 show the isobar lines in the porous bush and on the median plane position of the bearing for the power law index values which are equal to 0.9, 1 and 1.1 respectively and for the dimensionless permeability, $k=10^{-1}$.

Figures 26, 27 and 28 show the isobar lines in the porous bush and on the median plane position of the bearing for the power law index values which are equal to 0.9, 1 and 1.1 respectively and for the dimensionless permeability, $k=10^{-2}$.

Figures 29, 30 and 31 show the isobar lines in the porous bush and on the median plane of the bearing for the power law index values which are equal to 0.9, 1 and 1.1 respectively and for the dimensionless permeability, $k=10^{-3}$.

In all these figures, the dimensionless ratio, L/D_s, is maintained to be equal to 1. As it is shown in Figs. 6 and 7, the pressure concentration is observed in the angular position, $\theta=160°$.

It can be also noted that the increase in the power law index generates high pressure in the porous matrix.

In addition, all the figures illustrate that the increase in permeability generates a decrease in pressure in the porous bush.

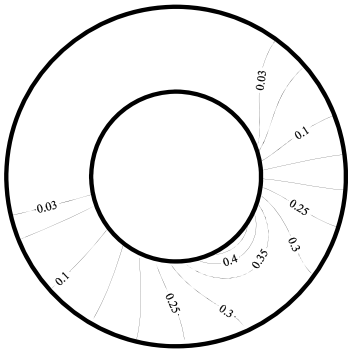

Fig. 23. Isobar lines on the median plane of the bearing for: $L/D_s=1$, n=0.9 and $k=10^{-1}$.

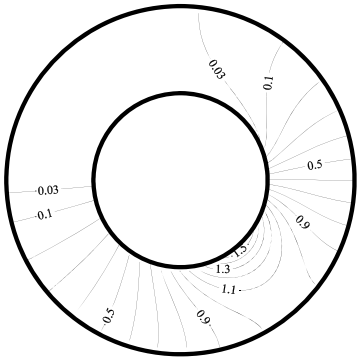

Fig. 24. Isobar lines on the median plane of the bearing for: $L/D_s=1$, n=1 and $k=10^{-1}$.

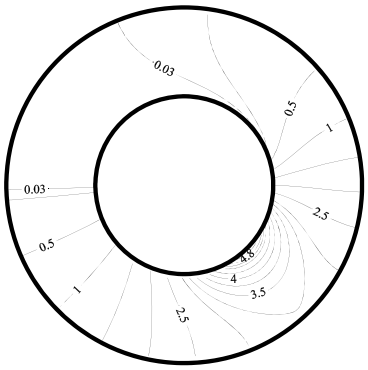

Fig. 25. Isobar lines on the median plane of the bearing for: $L/D_s=1$, n=1.1 and $k=10^{-1}$.

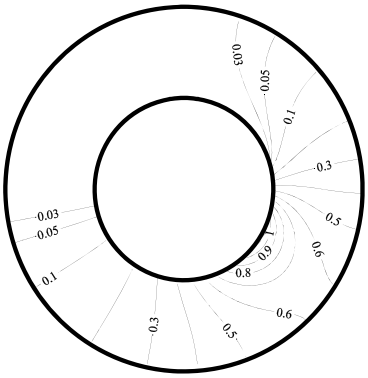

Fig. 26. Isobar lines on the median plane of the bearing for: $L/D_s=1$, n=0.9 and $k=10^{-2}$.

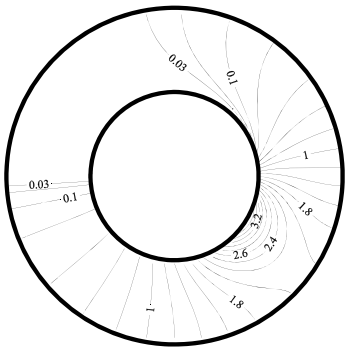

Fig. 27. Isobar lines on the median plane of the bearing for: $L/D_s=1$, n=1 and $k=10^{-2}$.

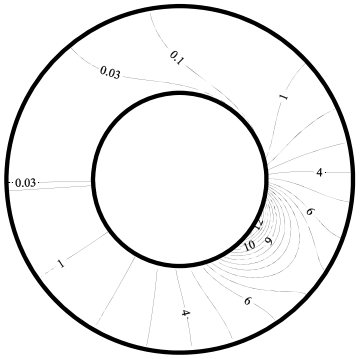

Fig. 28. Isobar lines on the median plane of the bearing for: $L/D_s=1$, n=1.1 and $k=10^{-2}$.

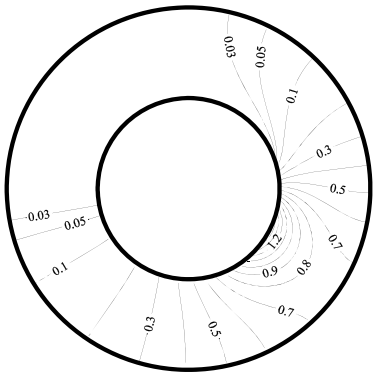

Fig. 29. Isobar lines on the median plane of the bearing for: $L/D_s=1$, n=0.9 and $k=10^{-3}$.

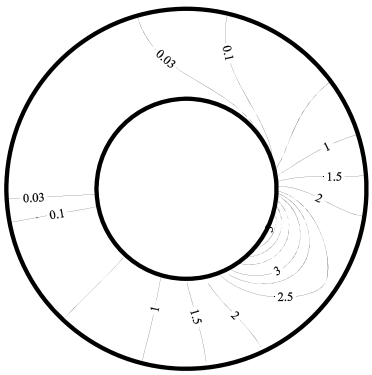

Fig. 30. Isobar lines on the median plane of the bearing for: $L/D_s=1$, n=1 and $k=10^{-3}$.

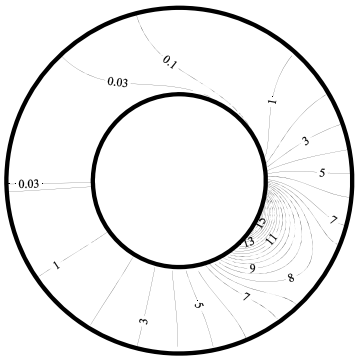

Fig. 31. Isobar lines on the median plane of the bearing for: $L/D_s=1$, $n=1.1$ and $k=10^{-3}$.

5. CONCLUSIONS

A numerical study based on hydrodynamic lubrication aspect analysis of porous journal bearings of finite length using non-Newtonian lubricant rheological behavior is done. The study is focused essentially on the effects of some parameters on the porous journal bearing characteristics. A computer program was developed to simulate the effect of the lubricant rheological behavior on these journal bearings characteristics.

Obtained results showed that:

1- The power law index, n, has important effects on the performance of porous and non-porous bearings.

2- The use of dilatant fluids can recover the degradation caused by the presence of the porous matrix.

3- The permeability has significant effects on the performance of porous journal bearings of finite length, in particular at higher eccentricity ratios. When the permeability increases, the maximum pressure and the load capacity decrease the friction factor and the attitude angle increases.

4- The increase in the relative eccentricity leads to an increase in the load capacity and a decrease in the attitude angle and coefficient of friction.

5- The increase of L/D_s ratio induces an increase in the pressure and load capacity.

6- Good agreement is observed between the results obtained in this study and those of literature revue (Mokhtar *et al*. (1984) and Ju *et al*. (1994)).

REFERENCES

Al-Fadhalah, K. J. and A. A. Elsharkawy (2008). Effect of non-Newtonian lubrication on the separation of a sphere from a flat, *Tribology International* 41, 1237–1246.

Balasoiu, A. M., M. J. Braun, S. I. Moldovan (2013). A parametric study of a porous self-circulating hydrodynamic bearing, *Tribology International* 61, 176–193.

Bhattacharjee, R. C. and N. C. Das (1996). Power law fluid model incorporated into elasto-hydrodynamic lubrication theory of line contact, *Tribology International* 29(5), 405-413.

Boubendir, S., S. Larbi, R. Bennacer (2010). A Contribution to the Analysis of the Thermo-Hydrodynamic Lubrication of Porous Self-Lubricating Journal Bearings,*Defect and Diffusion Forum* 297-301, 618–623.

Boubendir, S., S. Larbi, R. Bennacer (2011). Numerical study of the thermo-hydrodynamic lubrication phenomena in porous journal bearings, *Tribology International* 44, 1–8.

Braun, A. L. (1982). Porous bearings, *Tribology International* 15(5), 235-242, 1982.

Cameron, A. and V. T. Morgan (1957). Mechanism of lubrication in porous metal bearing, In: *Proceedings of the conference on lubrication and wear*, London, Great Britain 89, 151-157.

Christopherson, D. G. (1941). A new mathematical method for the solution of film lubrication problems, *Proc. I.M.E* 146, 126–135.

Chu, H. M., W. L. Li, Y. P. Chang (2006). Thin film elasto-hydrodynamic lubrication-a power-law fluid model, *Tribology International* 39, 1474 – 1481.

Darcy, H. (1856). *Les fontaines publiques de la ville de Dijon, Edition Dalmont*, Paris, France.

Elsharkawy, A. A. (2001). On the hydrodynamic liquid lubrication analysis of slider/disk interface, *International Journal of Mechanical Sciences* 43, 177–192.

Elsharkawy, A. A. and L. H. Guedouar (2001). Hydrodynamic lubrication of porous journal bearings using a modified Brinkman-extended Darcy model, *Tribology International* 34, 767–777.

Jang, J. Y. and C. C. Chang (1988). Adiabatic analysis of finite width journal bearings with non-Newtonian lubricants, *Wear* 122, 63 – 75.

Jang, J. Y. and C. C. Chang (1987). Adiabatic solutions for a misaligned journal bearing with non-Newtonian lubricants, *Tribology International* 20(5), 267-275.

Ju, S. M. and C. I. Weng (1994). Thermo-hydrodynamic analysis of finite-width journal bearings with non-Newtonian lubricants, *Wear* 171, 41-49.

Kango, S., R. K. Sharma, R. K. Pandey (2014), Thermal analysis of microtextured journal bearing using non-Newtonian rheology of lubricant and JFO boundary conditions. *Tribology International* 69, 19-29.

Lin J. F. and L. Y. Wang (1990). Thermo-hydrodynamic analysis of finite-width, partial-arc journal bearings with non-Newtonian lubricants: Part II, *Tribology International* 23(3), 211-216.

Lin, J. R., L. M. Chu, T. C. Hung, P. Y. Wang (2016). Derivation of two-dimensional non-Newtonian Reynolds equation and application to power-law film slider bearings: Rabinowitsch fluid model, *Applied Mathematical Modelling* 40(19-20), 8832–8841.

Mishra, P. C. (2013). Mathematical modeling of stability in rough elliptic bore misaligned journal bearing considering thermal and non-Newtonian effects, *Applied Mathematical Modelling* 37, 5896–5912.

Mokhtar, M. O. A., M. Raffat, G. S. A. Shawki (1984). Experimental investigations into the performance of porous journal bearings, *SAE paper*, No. 840097.

Mongkolwongrojn, M. and C. Aiumpronsin (2010). Stability analysis of rough journal bearings under TEHL with non-Newtonian lubricants, *Tribology International* 43, 1027-1034.

Naduvinamani, N. B. and S. Santosh (2011). Micropolar fluid squeeze film lubrication of finite porous journal bearing, *Tribology International* 44, 409–416.

Nessil, A., S. Larbi, H. Belhaneche and M. Malki (2013). Journal Bearings Lubrication Aspect Analysis Using Non-Newtonian Fluids, Advances in Tribology 213, 1- 9.

Prasad, D. and R. P. Chhabra (1991). Thermal and normal squeezing effects in lubrication of rollers by a power-law fluid, *Wear* 145, 61-76.

Rodin, G. J. (1996). Squeeze film between two spheres in a power-law fluid, *J Non-Newtonian Fluid Mech* 63, 141–152.

Sakim, A., M. Nabhani, M. E. L Khlifi (2018). Non-Newtonian effects on porous elastic journal bearings, *Tribology International* 120, 23- 33.

Sinha, P. and C. Singh (1981). Non-Newtonian squeeze films in spherical bearings, *Wear*, 68, 133–140.

Stieber, W. (1933). Das Schwimmlager. VDI, Berlin, Germany.

Swift, H. W (1932). The stability of lubricating films in journal bearings, *Proc. Inst. Civil Engineers*, UK 233, 267–288.

Vijaysri, M., R. P. Chhabra, V. Eswaran (1999). Power-law fluid flow across an array of infinite circular cylinders: a numerical study, *J.Non-Newtonian Fluid Mech* 87, 263–282.

Wang, S. H., D. Y. Hua, H. H. Zhang (1987). A full EHL solution for line contacts under sliding-rolling condition with a non-Newtonian rheological model, *Tribology Series* 11, 231-236.